Global Distribution of Large Lunar Craters: Implications for Resurfacing and Impactor Populations

James W. Head III, *et al.*

Science **329**, 1504 (2010);
DOI: 10.1126/science.1195050

Global Distribution of Large Lunar Craters: Implications for Resurfacing and Impactor Populations

James W. Head III,[1]* Caleb I. Fassett,[1] Seth J. Kadish,[1] David E. Smith,[2,3] Maria T. Zuber,[2,3] Gregory A. Neumann,[3] Erwan Mazarico[2,3]

By using high-resolution altimetric measurements of the Moon, we produced a catalog of all impact craters ≥20 kilometers in diameter on the lunar surface and analyzed their distribution and population characteristics. The most-densely cratered portion of the highlands reached a state of saturation equilibrium. Large impact events, such as Orientale Basin, locally modified the prebasin crater population to ~2 basin radii from the basin center. Basins such as Imbrium, Orientale, and Nectaris, which are important stratigraphic markers in lunar history, are temporally distinguishable on the basis of crater statistics. The characteristics of pre- and postmare crater populations support the hypothesis that there were two populations of impactors in early solar system history and that the transition occurred near the time of the Orientale Basin event.

The record of impact craters on the surface of the Moon, particularly the size-frequency distribution (SFD) and spatial density of craters, has long been used to infer information about the age of surfaces and the sequence of geological events (*1*). Unfortunately, uneven areal coverage, different image resolutions, and a wide range of solar illumination geometries from previous spacecraft mission data have precluded the compilation of a consistent global data set of the impact crater population. In the past year, the Lunar Orbiter Laser Altimeter (LOLA) (*2*), an instrument on board the Lunar Reconnaissance Orbiter (LRO) spacecraft, has acquired globally distributed, high-precision measurements of the topography of the Moon, which enable the creation of a 64-pixels-per-degree digital terrain model (DTM) and a shaded relief model of the surface (*3*). These data provide a view of the global distribution of impact craters without the observational uncertainties that arose from measurement of craters on images of heterogeneous illumination condition and uneven coverage and quality. We used this data set to produce a global compilation of the distribution of impact craters ≥20 km in diameter.

We mapped craters on the Moon by overlaying a 20-km reference grid on the topography and hillshade and by systematically measuring across the lunar surface (*4*) with the CraterTools extension to ArcMap (*5*) to make diameter measurements of craters. All craters with a measureable rim and central depression were cataloged, regardless of their degradation states or whether they were embayed or buried by younger surface

[1]Department of Geological Sciences, Brown University, Providence, RI 02912, USA. [2]Department of Earth, Atmospheric and Planetary Sciences, Massachusetts Institute of Technology, Cambridge, MA 02129, USA. [3]Solar System Exploration Division, NASA Goddard Space Flight Center, Greenbelt, MD 20771, USA.

*To whom correspondence should be addressed. E-mail: james_head@brown.edu

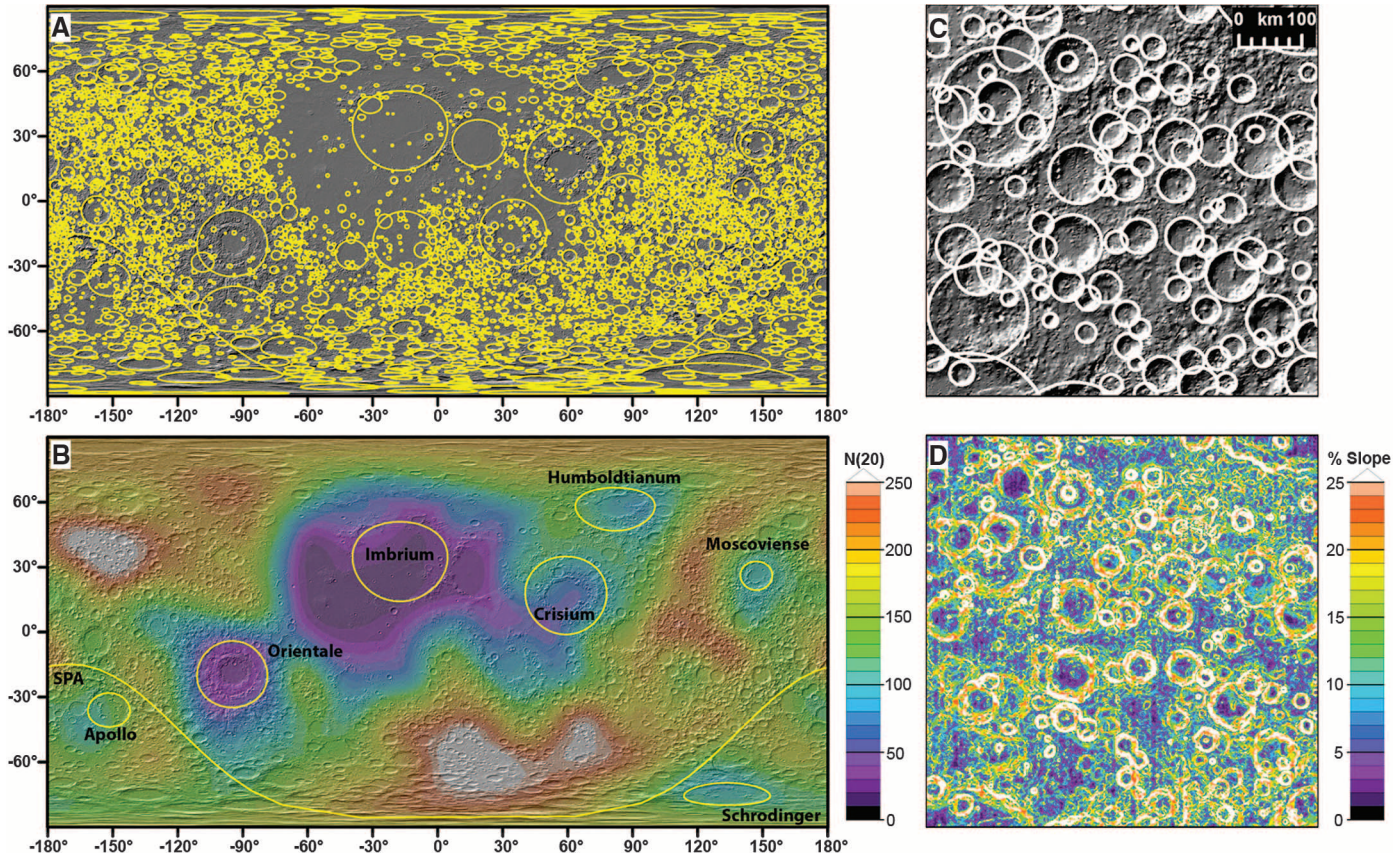

Fig. 1. (**A**) An outline of the craters mapped on the surface of the Moon from LOLA data superposed on a hillshade rendering of LOLA topography (*2*, *3*). (**B**) Crater densities on the Moon for craters ≥20 km in diameter, calculated in neighborhoods of radius 500 km. (**C** and **D**) Central far-side highlands (centered at −7°N, 130°E), one of the most densely cratered areas of the Moon. (C) Craters superposed on a LOLA hillshade base map. (D) Slope map of area in (C) showing the lack of smooth intercrater plains such as those found on Mercury (*11*).

units; identified craters were also examined in an underlying ArcMap layer containing the best available images. In total, we mapped 5185 craters with diameters ≥ 20 km on the lunar surface, a factor of ~2 increase in the number of craters of this size from Wilhelms *et al*. (*6*), whose analysis examined 82% of the lunar surface.

By using the craters mapped in our data set (Fig. 1A), we determined the areal density of craters on the Moon by calculating the number of craters in a moving neighborhood of 500 km in radius (Fig. 1B). The scale of this moving neighborhood sets the minimum area that is effectively sampled, ~8×10^5 km^2. The resulting crater densities reflect first-order variations in the crater retention age (for 20-km craters and larger) across the surface. We report densities here as $N(20)$ values, which represent the number of craters per unit area with diameter ≥ 20 km, normalized to 10^6 km^2. The most prominent features in Fig. 1B are (i) the densely cratered highlands, particularly on the southern nearside and north-central far side of the Moon, (ii) the interior and surroundings of stratigraphically young impact basins, especially Orientale, and (iii) mare regions, which have the lowest crater densities on the Moon.

Impact crater SFD analyses for units in the maria have been used successfully to develop stratigraphic sequences for individual areas (*7*) and combined with radiometric dates from samples returned from the lunar maria to establish a volcanic flux for the Moon as a whole (*8*). These SFD techniques can thus link specific mare crustal units to relative and absolute ages. For the highlands, on the other hand, crater densities are in the range $N(20)$ = 100 to 280. These extremely high densities in the highlands are important because they fall in a range of ~3 to 10% of geometric saturation (*9*), consistent with empirical saturation equilibrium (*10*), a condition where, on average, every new crater erases a preexisting crater of comparable size. Because nearly all of the lunar highlands are in this range, our data further demonstrate that impact crater SFDs, unlike those in the younger maria, do not directly reflect differences in the actual age of the underlying crustal rocks. Examples of the most densely cratered surfaces on the Moon (Fig. 1C) illustrate this well: Crater densities in the north-central far side are so high that addition of new craters over most of the size range does not measurably change the SFD (and thus the age), despite the fact that the crustal rocks themselves are likely to date from

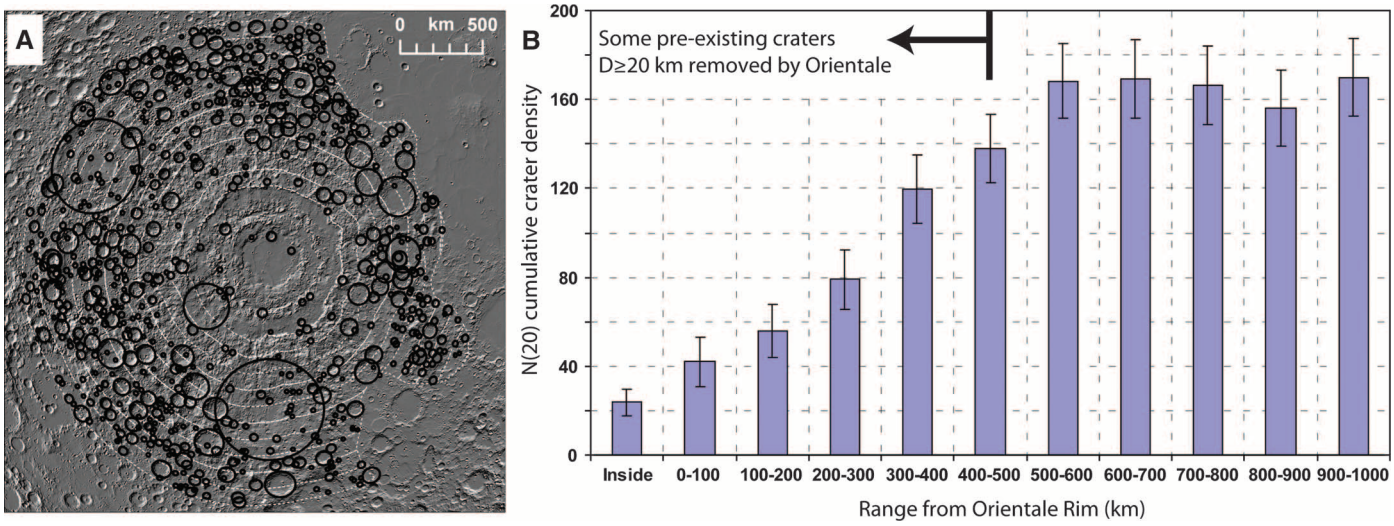

Fig. 2. Orientale Basin and radial distribution of craters. (**A**) Distribution of craters in the surroundings of Orientale on LOLA hillshade base map. (**B**) $N(20)$ cumulative crater density as a function of increasing radial range from the Orientale basin center. Error bars in all figures are $\sigma \pm \sqrt{N}/A$, where A is the count area.

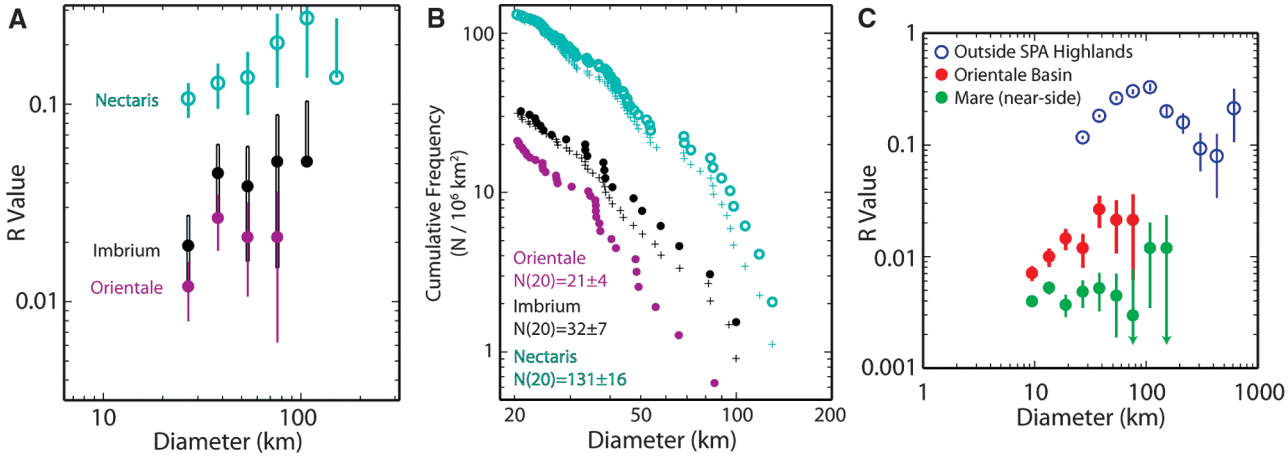

Fig. 3. Crater size-frequency distributions. (**A**) R plot (*21*) and (**B**) cumulative plot of craters superposed on three important basin stratigraphic markers on the Moon, which are clearly separable in crater density. On the cumulative plot, for mare-filled basins Imbrium and Nectaris, relevant counts areas are computed in two ways that give a similar qualitative results: a traditional rim-area method [circles, also the data in (B)] and with a buffered crater counting correction (*16*) that allows inclusion craters on the margin of the mare that superpose the basin (hatches). (**C**) R plot (areal density) (*21*) of craters superposed on lunar nearside mare, Orientale, and representative highlands crust (outside South Pole–Aitken Basin), which illustrates the difference in density and SFD slope on these terrains (*18*).

the most ancient period of lunar crustal genesis, a few hundred million years after lunar formation. Furthermore, slope maps of this area (Fig. 1D) show no evidence for extensive smooth areas such as intercrater plains, the type of volcanic resurfacing thought to have accompanied the early crustal history of Mercury (*11*). Such early volcanism could have occurred on the Moon (*12*) but is not now detectable by using SFD data because of crater saturation equilibrium. Conversely, these observations demonstrate that extrusive volcanism in early lunar history, if it occurred, was characterized by a flux low enough that it did not influence the crater population in a detectable manner.

Examination of the highlands impact crater density distribution (Fig. 1, A and B) does show regional variations, however. The interior and surroundings of stratigraphically young impact basins, especially Orientale, show $N(20)$ numbers intermediate between the most heavily cratered highlands [$N(20)$ = 150 to 250] and the lunar maria [$N(20)$ = 25 to 50]. These data show that the proximity of a given region to young craters and basins was a key factor in establishing the local variations in crater density that is observed. This phenomenon results from the obliteration of craters below the impact basin itself, the burial of craters near the basin rim [in a process described as proximity weathering or degradation (*13*)], and their modification further away, by the dynamic emplacement of the basin ejecta. This process, proximity age resetting, results in selective loss of craters of different diameters as a function of the basin size and increasing radial range. For example, the formation of the 930-km-diameter Orientale Basin (Figs. 1B and 2A) resulted in the complete obliteration of craters below the basin (an area of 6.8×10^5 km^2), and the demonstrable loss of craters ≥20 km diameter out to about 500-km radius from the basin rim crest (Fig. 2B). Within 100 km of the basin rim crest, the $N(20)$ number decreased by ~74% compared with the regional background population, between 100 and 300 km by ~60% and between 300 to 500 km by ~19%, before returning to the regional average of ~$N(20)$ = 160 at radial distances greater than ~500 km from the rim crest (Fig. 2B). Thus, detailed examination of the Orientale crater population (Figs. 1 and 2) shows that this single basin-forming event significantly altered the preexisting crater population, causing proximity age resetting out to a radial range of ~965 km from the basin center, an area comprising ~8% of the total lunar surface. Furthermore, analysis of Fig. 1B in the vicinity of Orientale Basin shows low-density lobes extending to the south over Mendel-Rydberg Basin and to the northwest toward Hertzsprung Basin, both of which predate Orientale but are relatively young stratigraphically.

In addition to obliterating craters, impact basin events also create large secondary craters at radial distances in excess of about one basin radius from the rim crest. These craters are predicted to be ~4% of the size of the primary (*14*) and known to range up to diameter (D) ~ 25 km for Orientale Basin (*1*). Thus, basins larger than Orientale could have produced even larger secondary craters and crater clusters. Indeed, basin secondary craters up to 20 to 40 km in diameter have been hypothesized to be an important part of the highland crater population, potentially polluting the primary impactor population and skewing surfaces to artificially older ages (*15*). To test this hypothesis, we performed an analysis similar to that shown in Fig. 2 for Orientale (D = 930 km), Imbrium (D = ~1160 km) and South Pole–Aitken (D ~ 2500 km) basins, centering the count areas on each basin and extending the annular analysis out to one basin diameter from the rim crest, an area known to contain radial ejecta and secondary crater chains and fields (*1*). As can be seen in the Orientale example (Fig. 2), the $N(20)$ values for the range between 500 and 1000 km from the rim crest are similar to the $N(20)$ values for typical, but not the most densely cratered, highlands (Fig. 1B). Similar relationships are seen for Imbrium and South Pole–Aitken basins. No annular zones of statistically significant increased crater density are observed, nor do secondaries traceable to these basins appear to contribute a significant number of craters ≥20 km to the crater population of surrounding regions.

We used the global crater database to revisit the SFD of important basins (Orientale, Imbrium, and Nectaris) that represent important markers within the lunar stratigraphy (*1*) and determined the superposed crater populations on these three basins (Fig. 3, A and B). Not surprisingly, the SFD plots (both R and cumulative) show a clear, separable distinction between these three basins, with Orientale and Imbrium being closer together in crater frequency than Imbrium and Nectaris. Our global data set, however, permits the use of buffered crater-counting techniques (*16*), and this results in a more robust SFD to be determined for these three important stratigraphic markers (see crosses in Fig. 3B). This enables a reanalysis of the sequence of basins proposed by Wilhelms (*1*) to lie between, and before, these key events. Further, should absolute age dates of key basin events be firmly established, these data will permit a more robust determination of the flux in early lunar history, and a test of the late heavy bombardment hypothesis (*17*).

Controversy has long existed concerning the nature of the impactor population bombarding inner planetary body surfaces throughout solar system history. Some hypothesize that the impactor population has been essentially similar in source and makeup throughout history, differing only in flux (*18*). Others have suggested that there is a clear difference in the populations with time and that this difference is reflected in the shape of the SFD of older and younger crater populations seen on planetary surfaces (*6*, *19*). The global data set permits the assessment and testing of these hypotheses. For Orientale and the nearside mare, both of which are geologically young, we have extended our crater database to a minimum diameter of D = 8 km and examined stratigraphic relationships to ensure that measured craters are superposed on (postdate) these features.

Our data show a distinct difference between the shape of the SFD of the older highland and younger mare crater populations (Fig. 3C). The highlands have a greater density of large craters (D ~ 50 to 100 km) compared with small craters (e.g., D ~ 20 to 30 km) than the mare surfaces. This is consistent with a less-steep production function at this size range. We applied the two-sample Kolmogorov-Smirnov test to assess the formal significance of this apparent difference in the shape of crater SFD on these units and found a very low probability that these SFD are the same distribution ($P \sim 1.5 \times 10^{-9}$). This difference is evident in our data both in the highlands as a whole, as well as in "pure" subregions of the highlands (*20*), which have been suggested as examples of the least modified cratered regions of the lunar crust. The SFD distribution of craters superposed on Orientale may be intermediate in nature, although it is statistically not distinguishable from the mare. These global observations show a change in the lunar SFD, consistent with observations on less comprehensive lunar data sets (*6*, *19*). This supports the conclusions of Strom *et al*. (*19*), who hypothesized the existence of an early and a later impactor population inside the asteroid belt. Furthermore, it places the transition between these two populations at about the time of Orientale Basin, the last large multi-ringed basin thought to have formed ~3.8 billion years ago (*1*).

References and Notes

1. D. E. Wilhelms, *The Geologic History of the Moon* (U.S. Geological Survey Professional Paper no. 1348, Washington, DC, 1987).
2. D. E. Smith *et al*., *Space Sci. Rev.* **150**, 209 (2010).
3. D. E. Smith *et al*., *Geophys. Res. Lett.*, in press; available online at www.agu.org/journals/pip/gl/2010GL043751-pip.pdf.
4. Crater diameter measurements using the CraterTools extension (*3*) are defined on the basis of a best-fit circle, fit to the crater rim based on three points selected along the rim or, alternatively, based on drawing a rim-to-rim diameter. CraterTools corrects measurements to a local map projection. Regions poleward of 70° latitude are examined separately in polar projections, and these data are then merged with the mid- and low-latitude data to produce the global data set. This survey method is repeated at multiple scales to ensure that all craters were detected, from the basins to 20-km-scale craters.
5. T. Kneissl *et al*., *Planet. Space Sci.*, in press; published online 24 March 2010 (10.1016/j.pss.2010.03.015).
6. D. E. Wilhelms *et al*., *Proc. Lunar Sci. Conf.* **IX**, 3735 (1978).
7. H. Hiesinger, R. Jaumann, G. Neukum, J. W. Head III, *J. Geophys. Res.* **105**, 29,239 (2000).
8. H. Hiesinger *et al*., *J. Geophys. Res.* **108**, 5065 (2003).
9. D. E. Gault, *Radio Sci.* **5**, 273 (1970).
10. J. E. Richardson, *Icarus* **204**, 697 (2009).
11. R. G. Strom, N. J. Trask, J. E. Guest, *J. Geophys. Res.* **80**, 2478 (1975).
12. J. W. Head III, L. Wilson, *Geochim. Cosmochim. Acta* **56**, 2155 (1992).
13. J. W. Head, *Moon* **12**, 299 (1975).
14. H. J. Melosh, *Impact Cratering* (Oxford, New York, 1989).
15. D. E. Wilhelms, *Proc. Lunar Sci. Conf.* **VII**, 2883 (1976).

16. C. I. Fassett, J. W. Head III, *Icarus* **195**, 61 (2008).
17. B. A. Cohen, T. D. Swindle, D. A. Kring, *Science* **290**, 1754 (2000).
18. G. Neukum, B. A. Ivanov, W. K. Hartmann, *Space Sci. Rev.* **96**, 55 (2001).
19. R. G. Strom, R. Malhotra, T. Ito, F. Yoshida, D. A. Kring, *Science* **309**, 1847 (2005).
20. W. K. Hartmann, *Meteoritics* **30**, 451 (1995).
21. *R* plots are constructed by dividing the differential SFD by a power law $dN/dD \sim D^{-3}$, where *N* is the number of craters within a given increment of crater diameter in a given area (*18*).
22. We thank the LRO and LOLA mission teams for their efforts, which made the observations in this study possible, and T. Kneissl for developing the CraterTools extension to ArcMap. Funding was provided by NASA grant NNX09AM54G for LOLA.

13 July 2010; accepted 25 August 2010
10.1126/science.1195050

Global Silicate Mineralogy of the Moon from the Diviner Lunar Radiometer

Benjamin T. Greenhagen,[1]* Paul G. Lucey,[2] Michael B. Wyatt,[3] Timothy D. Glotch,[4] Carlton C. Allen,[5] Jessica A. Arnold,[4] Joshua L. Bandfield,[6] Neil E. Bowles,[7] Kerri L. Donaldson Hanna,[3] Paul O. Hayne,[8] Eugenie Song,[6] Ian R. Thomas,[7] David A. Paige[8]

We obtained direct global measurements of the lunar surface using multispectral thermal emission mapping with the Lunar Reconnaissance Orbiter Diviner Lunar Radiometer Experiment. Most lunar terrains have spectral signatures that are consistent with known lunar anorthosite and basalt compositions. However, the data have also revealed the presence of highly evolved, silica-rich lunar soils in kilometer-scale and larger exposures, expanded the compositional range of the anorthosites that dominate the lunar crust, and shown that pristine lunar mantle is not exposed at the lunar surface at the kilometer scale. Together, these observations provide compelling evidence that the Moon is a complex body that has experienced a diverse set of igneous processes.

Remote characterization of mineralogy through thermal emission spectroscopy has a long history in planetary science that recently has been highlighted by global maps of martian mineralogy obtained from orbit and measurements from the martian surface (*1*, *2*). Although infrared emission spectroscopy is sensitive to the bulk composition and can readily identify important lunar silicates such as feldspar, pyroxene, olivine, and quartz (*3*), earlier lunar observations (*4*, *5*) lacked sufficient spatial resolution or coverage to identify areas that may have escaped extensive physical mixing and retain unusual lithologies. High-resolution lunar mapping has thus far been limited to visible and near-infrared spectroscopy and multispectral imaging, which have been used to identify diverse compositions over large areas of the lunar surface (*6*–*9*). However, these techniques are relatively insensitive to nominally iron-free minerals such as quartz and feldspar and can only unambiguously detect the important lunar rock–type anorthosite in exposures that contain almost no mafic minerals, such as pyroxene or olivine (*9*). Multispectral thermal emission data from the Diviner lunar radiometer have high spatial resolution, near global coverage, and sensitivity to important iron-poor mineralogy.

Launched onboard the Lunar Reconnaissance Orbiter (LRO) in June 2009, Diviner is a nine-channel pushbroom mapping radiometer that measures emitted thermal radiation (seven channels) and reflected solar radiation (two channels) between 0.3 and 400 μm at a spatial resolution of approximately 200 m (*10*). The Diviner compositional investigation relies primarily on the three shortest wavelength thermal infrared channels near 8 μm: 7.55 to 8.05 μm, 8.10 to 8.40 μm, and 8.38 to 8.68 μm. Pioneering lunar mid-infrared spectroscopic studies, including airborne (*4*), ground-based (*5*), and laboratory (*11*–*13*) measurements, have shown this region is key to identifying common lunar silicate minerals, and the Diviner compositional investigation was designed by using the results of those studies (*14*).

We chose Diviner's 8-μm-region channels to characterize a well-studied compositional indicator of silicate mineralogy called the Christiansen feature (CF) (*14*, *15*). The wavelength position of CF is strongly dependent on the degree of polymerization of minerals, with framework silicate minerals such as feldspars exhibiting CFs at shorter wavelengths than less polymerized pyroxene and olivine (*3*, *16*, *17*). Common lunar minerals thus exhibit widely separated CF positions. The CF position of soils is close to the weighted average of the constituent minerals, which enables determination of major lunar lithologies (*18*). The presence of strong thermal gradients in the lunar environment causes systematic shifts in CF position and an enhancement of CF spectral contrast relative to other mid-infrared features, such as Reststrahlen bands (*3*, *19*, *20*). Therefore, lunar thermal emission observations are only directly comparable with laboratory emission measurements in a simulated lunar environment (*21*, *22*).

We used ~10^8 three-point 8-μm-region spectra collected between 5 August 2009 and 24 November 2009, covering ~50% of the lunar surface

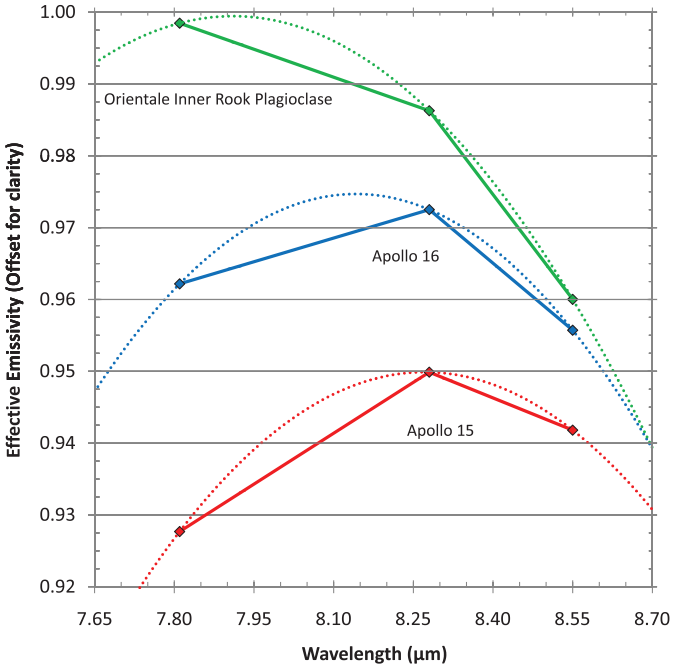

Fig. 1. Diviner 8-μm-region channel three-point spectra representing typical spectral variability. The CF position was determined by using a parabolic fit to the three points (dotted traces).

[1]Jet Propulsion Laboratory, California Institute of Technology, Pasadena, CA 91109, USA. [2]Hawaii Institute of Geophysics and Planetology, University of Hawaii, Honolulu, HI 96822, USA. [3]Department of Geological Sciences, Brown University, Providence, RI 02912, USA. [4]Department of Geosciences, Stony Brook University, Stony Brook, NY 11794, USA. [5]NASA Johnson Space Center, Houston, TX 77058, USA. [6]Department of Earth and Space Sciences, University of Washington, Seattle, WA 98195, USA. [7]Department of Atmospheric, Oceanic, and Planetary Physics, Oxford University, OX1 3PU Oxford, UK. [8]Department of Earth and Space Sciences, University of California, Los Angeles, Los Angeles, CA 90095, USA.

*To whom correspondence should be addressed. E-mail: benjamin.t.greenhagen@jpl.nasa.gov